EurJIC
European Journal of Inorganic Chemistry

Research Article
doi.org/10.1002/ejic.202200149

Chemistry Europe
European Chemical Societies Publishing

www.eurjic.org

Suitability of Carbazolyl Hauser and Turbo-Hauser Bases as Magnesium-Based Electrolytes

Philipp Schüler[+],[a] Simon Sengupta[+],[a] Steve Zaubitzer,[b] Florian Fiesinger,[c] Saustin Dongmo,[b] Helmar Görls,[a] Margret Wohlfahrt-Mehrens,[b, d] Matthias van den Borg,[c] Daniel Gaissmaier,[c, d, e] Sven Krieck,[a] Mario Marinaro,[b] Timo Jacob,[c, d, e] and Matthias Westerhausen*[a]

Lithium-ion batteries pose certain drawbacks and alternatives are highly demanded. Requirements such as low corrosiveness, electrochemical stability and suitable electrolytes can be met by magnesium-ion batteries. Metalation of carbazole with Mg in THF in the presence of ethyl bromide yields the sparingly soluble Hauser base [(thf)$_3$Mg(Carb)Br] (**1**) which shows a Schlenk-type equilibrium with formation of [(thf)$_3$Mg(Carb)$_2$] and [(thf)$_4$MgBr$_2$]. A THF solution of **1** shows a low overpotential and a good cyclability of electrodeposition/-stripping of Mg on a Cu current collector. An improved performance is achieved with the turbo-Hauser bases [(thf)(Carb)Mg(μ-Br/X)$_2$Li(thf)$_2$] (X = Br (**2**) and Cl (**3**)) which show a significantly higher solubility in ethereal solvents. The THF solvation energies increase from (thf)$_x$MgBr$_2$ over (thf)$_x$Mg(Carb)Br to (thf)$_x$Mg(Carb)$_2$ for an equal number x of ligated THF molecules.

Introduction

Hauser bases are magnesium amide bases that have been described firstly by Hauser and Walker in 1947.[1] These bases represent valuable and often chemoselective metalation reagents.[2] Commonly Hauser bases R$_2$N–Mg(L)–X crystallize as dimeric complexes with bridging halide[3] or amido ligands.[3b,4] In solution, quite complex temperature-dependent Schlenk-type equilibria between mono- and dinuclear complexes on the one hand and homo- and heteroleptic compounds on the other have been elucidated for *i*Pr$_2$N–MgCl in THF solution based on DOSY-NMR experiments.[5] The addition of lithium halide produces the turbo-Hauser bases (Knochel-Hauser reagents) of the general type R$_2$N–MgCl·LiCl with enhanced reactivity and chemoselectivity.[6] Expectedly, equilibria between diverse species have been observed in solution by DOSY-NMR spectroscopy.[5,7] The preparation of these turbo-Hauser bases proceeds smoothly by deprotonation of secondary amines with Grignard reagents in the presence of lithium halide or with turbo-Grignard reagents such as *i*PrMgCl·LiCl.[8]

Besides the widely used application of Hauser and turbo-Hauser bases as selective metalation reagents, we are interested in magnesium batteries.[9] Not only the nature of the electrodes[10] plays an important role, but also the electrolyte causes challenges that have to be addressed beyond aqueous systems.[11]

The realization of zero-emission is one of the greatest challenges of our generation. For the transformation from classical fossil-based transportation to a fully electrical one, lithium-ion-batteries (LIBs) are nowadays the only choice due to their outstanding energy performance. Nevertheless, raw materials for LIBs are not available in unlimited quantities and therefore might not cover the increasing demand for electrochemical storage.[12] Furthermore, dendrite growth at the surface of Li metal and side reactions with the electrolyte pose challenges.[13] This has led scientists around the world to search for alternatives to today's established technologies.[14] Magnesium (Mg) possesses the highest volumetric capacity (3833 mAh cm^{-3}) compared to calcium (Ca) (2073 mAh cm^{-3}), lithium (Li) (2062 mAh cm^{-3}), and sodium (Na) (1128 mAh cm^{-3}) and furthermore, the high abundance makes a Mg-based battery as a promising candidate to opening up the post-lithium age. Since the realization of the first Mg battery by

[a] P. Schüler,[+] S. Sengupta,[+] Dr. H. Görls, Dr. S. Krieck, Prof. Dr. M. Westerhausen
Institute of Inorganic and Analytical Chemistry
Friedrich Schiller University Jena (FSU)
Humboldtstraße 8, 07743 Jena, Germany
E-mail: m.we@uni-jena.de
www.westerhausen.uni-jena.de
[b] S. Zaubitzer, Dr. S. Dongmo, Dr. M. Wohlfahrt-Mehrens, Dr. M. Marinaro
Zentrum für Sonnenenergie und Wasserstoff-Forschung Baden-Württemberg
Helmholtzstraße 8, 89081 Ulm, Germany
[c] F. Fiesinger, M. van den Borg, D. Gaissmaier, T. Jacob
Institute of Electrochemistry
University Ulm
Albert-Einstein-Allee 47, 89081 Ulm, Germany
[d] Dr. M. Wohlfahrt-Mehrens, D. Gaissmaier, T. Jacob
Helmholtz Institute Ulm (HIU) Electrochemical Energy Storage
Helmholtzstraße 11, 89081 Ulm, Germany
[e] D. Gaissmaier, T. Jacob
Karlsruhe Institute of Technology (KIT)
P.O. Box 3640, D-76021 Karlsruhe, Germany
[+] These authors contributed equally to this publication.

Supporting information for this article is available on the WWW under https://doi.org/10.1002/ejic.202200149

Research Article
doi.org/10.1002/ejic.202200149

using a Chevrel Phase (CP) as cathode and moreover the compatibility with a sulfur (S) cathode, the research activities onto the development of Mg-based electrolytes and appropriate electrolyte compatible electrode materials have been increased over time.[15]

Results and Discussion

Synthesis of Carbazolyl Magnesium Bromide

For the use as an electrolyte in magnesium batteries, specific requirements must be fulfilled such as low corrosiveness, electrochemical stability, straightforward synthesis, and high solubility in suitable solvents. Therefore, we studied the carbazolyl Hauser and turbo-Hauser bases. The direct magnesiation of carbazole by magnesium turnings is impossible. Therefore, we applied the *in-situ* Grignard metalation method (*i*GMM)[16] and added ethyl bromide to a suspension of carbazole and magnesium turnings in THF at room temperature as depicted in Scheme 1. Toward the end of the metalation reaction, carbazolyl magnesium bromide [(thf)$_3$Mg(Carb)Br] (**1**) crystallized from the reaction mixture in the shape of slightly greenish blocks. A Schlenk-type equilibrium between heteroleptic CarbMgBr on the one hand and homoleptic Mg(Carb)$_2$ and MgBr$_2$ on the other was observed in [D$_8$]THF solution by NMR spectroscopy (cf. Figures S1-S4). DOSY-NMR experiments verify the mononuclear nature of the magnesium amide complexes (cf. Figure S5).

The *i*GMM was performed in the presence of LiBr and of LiCl yielding the corresponding heterobimetallic turbo-Hauser bases as shown in Scheme 1 (for NMR cf. Figures S6-S10 and Figure S12). DOSY-NMR investigations supported the composition of 1:1 adducts of the type (Carb)MgLiBrX (X = Br (**2**), Cl (**3**)) (cf. Figure S11). The solubility significantly increased in the order **1** < **2** < **3**, and in fact, crystalline [(thf)$_3$Mg(Carb)Br] (**1**) is very sparingly soluble even in ethereal solvents.

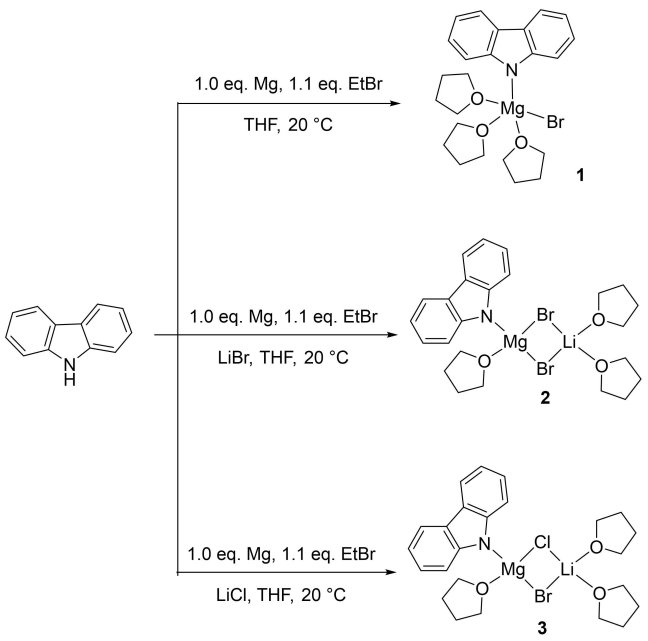

Scheme 1. Synthesis of thf adducts of the carbazolyl magnesium bromide (**1**, carbazolyl Hauser base) as well as its lithium bromide (**2**) and lithium chloride (**3**) adducts (carbazolyl turbo-Hauser bases).

Solid-State Structure

The molecular structure and atom labeling scheme of [(thf)$_3$Mg(Carb)Br] (**1**) are depicted in Figure 1. The magnesium atom Mg1 is in a trigonal bipyramidal environment with the two thf ligands of O1 and O3 in apical positions. The Mg1–N1 bond length of 204.5(3) pm is significantly larger than the Mg-N distances in dinuclear [(TMP)Mg(thf)(μ-Cl)]$_2$ (198.1(2) pm) and [(thf)$_2$Li(μ-Cl)$_2$Mg(thf)(TMP)] (195.58(14) pm)[3b] which is primarily a consequence of the larger coordination number of the magnesium center.

Electrochemical Study

Efficient metal deposition and stripping are crucial for operating metal-based batteries. Therefore, the reversibility of the electrodeposition and electro-stripping of Mg metal in the novel carbazolyl-based electrolyte was investigated using cyclic voltammetry (CV). Figure 2a shows the features of electrodeposition/-stripping of Mg metal on a Cu current collector. At cycle #10, the over-potential for Mg deposition was −330 mV

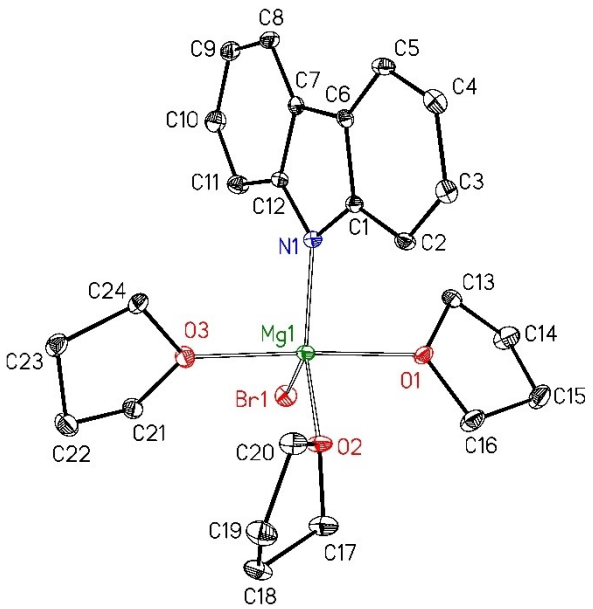

Figure 1. Molecular structure and atom labelling scheme of [(thf)$_3$Mg(Carb)Br] (**1**). The ellipsoids represent a probability of 30%, H atoms are neglected for the sake of clarity. Selected bond lengths (pm): Mg1–N1 204.5(3), Mg1–Br1 250.81(11), Mg1–O1 209.6(2), Mg1–O2 206.5(2), Mg1–O3 213.1(2); bond angles (deg.) at Mg1: N1—Mg1—Br1 125.65(9), N1–Mg1–O1 89.49(10), N1–Mg1–O2 120.62(11), N1–Mg1–O3 91.65(10), O1–Mg1–O2 87.44(10), O1–Mg1–O3 173.87(11), O1–Mg1–Br1 91.89(7), O2–Mg1–O3 86.80(10), O2–Mg1–Br1 113.72(8), O3–Mg1–Br1 92.34(7).

Research Article
doi.org/10.1002/ejic.202200149

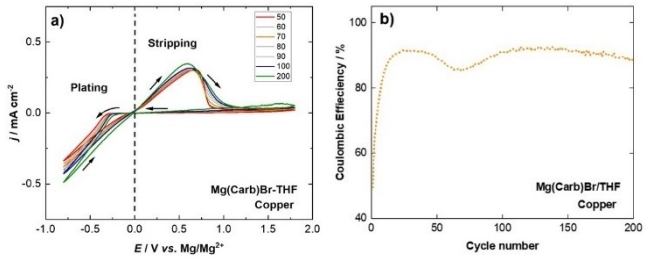

Figure 2. (a) Cyclic voltammograms of magnesium electro-deposition/electro-stripping on a Cu current collector using 0.26 M [$(thf)_3Mg(Carb)Br$] (**1**) in THF. Scan rate: 10 mV s^{-1}. RE/CE: Magnesium metal. (b) Respective Coulombic efficiency from cyclic voltammetry measurement.

vs. Mg/Mg^{2+} and further decreases down to −220 mV *vs.* Mg/Mg^{2+} at cycle #200th. The low over-potential and cyclability is a substantial improvement over the borate-based $Mg[B(hfip)_4]_2$/DME (~400 mV) and $B(OMgCl)_3$/Triglyme and Triglyme/THF (> 500 mV) electrolytes.[17] The Coulombic efficiency for the electro-deposition/-stripping process of Mg metal is close to 91 % (cf. Figure 2b).

This novel electrolyte formulation shows an increase in the electrolyte stability of 500 mV as in contrast to the reported stabilities of 1.5 V for Grignard-based electrolytes; it is for copper and stainless steel more than 2 V (cf. Figure S18).[18] The electrochemical performance in terms of cathodic and anodic current densities, which corresponds to the electro-deposition/-stripping process, respectively, and efficiency can be further improved with the addition of LiCl (cf. Figure S19). This might be due to the activation of the Mg surface by the chlorine-anion or either to the formation of a Li-contained Solid Electrolyte Interface (SEI).[19] The electro-deposited material on Cu current collector was characterized by XRD and SEM techniques. Figure 3b shows the XRD pattern of Mg metal deposited on the Cu current collector. The reflection patterns can be clearly assigned to a hexagonal Mg structure and to the Cu current collector (substrate).[20] Figure 3a shows that the Mg electro-deposited as compact particles with different orientations. Elemental analysis of the deposited material via EDX measurement confirmed the XRD findings of deposited Mg (cf. SI Figure S20).

The morphology of the electro-deposited Mg is influenced by the electrolyte composition. In the presence of LiCl, the Mg electro-deposited patchier (cf. Figure S21).

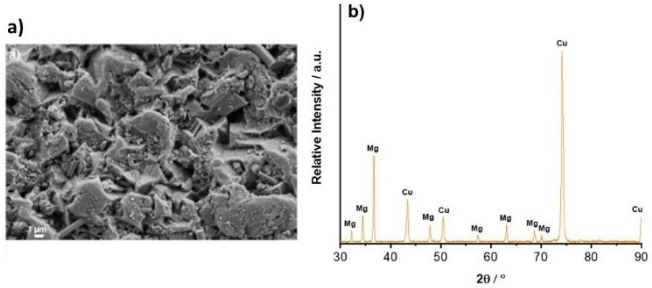

Figure 3. (a) Scanning electron micrograph of electro-deposited magnesium on copper current collector (magnification = 10.000-fold). (b) Respective XRD patterns of the electro-deposited magnesium obtained after chronopotentiometry at −0.6 mA cm^{-2}.

Computational Study

Density functional theory (DFT) calculations were performed to determine the solvation energies and Mulliken charges for $(thf)_xMgCarbBr$, $(thf)_xMg(Carb)_2$, and $(thf)_xMgBr_2$ at different degrees of solvation ($x \hat{=}$ number of coordinated THF molecules). As the degree of solvation increases, the structure of the electrolyte changes from a linear ($x = 0$) via a trigonal-planar ($x = 1$) to a tetrahedral ($x = 2$) via a trigonal-bipyramidal ($x = 3$) to an octahedral complex ($x = 4$), as shown in Table S1 (see Supporting Information). Table 1 summarizes the energy gain per additional THF molecule ($E_{solv,gain}$) as well as the cumulative solvation energy ($E_{solv,cum}$) for the corresponding conformation. The contribution to the solvation energetics per additional THF decreases, as expected, with an increasing degree of solvation. For example, the gain in solvation energy for Mg(Carb)Br is −148 kJ·mol^{-1} for the first, −125 kJ·mol^{-1} for the second, −94 kJ·mol^{-1} for the third, and −64 kJ·mol^{-1} for the fourth THF molecule. The cumulative solvation energies for a given degree of solvation are the highest for $Mg(Carb)_2$, followed by Mg(Carb)Br and $MgBr_2$. Following this order, the cumulative solvation energies for 3 coordinated THF molecules are −403 kJ·mol^{-1}, −367 kJ·mol^{-1}, and −336 kJ·mol^{-1}, respectively. This finding already indicates that the bromide ligand provides more negative charge to the Mg cation than the carbazolyl group, which would explain the stronger bonding between the central magnesium cation and the oxygen of THF for $Mg(Carb)_2$. We further see that the HOMO and LUMO energy levels increase (i.e. become less negative) with higher solvation degrees, as shown in Table 2. Since lower HOMO levels of the electrolyte correspond to better anodic stability, we expect a diminished oxidative stability with increasing THF solvation.[21]

The Mulliken charge analysis for MgCarbBr in Figure 4 indicates a decrease in negative charge on the THF oxygen atoms of approximately 4 % per additional THF molecule. This is caused by the lower individual contribution of each THF to donate negative charge to the magnesium cation. An increasing

Table 1. Solvation energy gain $E_{solv,gain}$ and cumulative solvation energy $E_{solv,cum}$ in kJ·mol^{-1} of heteroleptic $(thf)_xMgCarbBr$ and homoleptic $(thf)_xMg(Carb)_2$, as well as $(thf)_xMgBr_2$ at varying degrees of solvation (x = number of ligated THF molecules). Due to steric effects, a maximum of 3 THF molecules could be coordinated to $Mg(Carb)_2$. The total energies used for calculating $E_{solv,gain}$ and $E_{solv,cum}$ are given in Table S2 (see Supporting Information).

x	$(thf)_xMg(Carb)Br$		$(thf)_xMg(Carb)_2$		$(thf)_xMgBr_2$	
	$E_{solv,gain}$	$E_{solv,cum}$	$E_{solv,gain}$	$E_{solv,cum}$	$E_{solv,gain}$	$E_{solv,cum}$
1	−148	−148	−164	−164	−132	−132
2	−125	−273	−147	−311	−117	−249
3	−94	−367	−92	−403	−87	−336
4	−63	−430	–	–	−79	−414

Research Article
doi.org/10.1002/ejic.202200149

Table 2. HOMO and LUMO energy levels in eV of heteroleptic $(thf)_xMgCarbBr$ and homoleptic $(thf)_xMg(Carb)_2$, as well as $(thf)_xMgBr_2$ at varying degrees of solvation (x = number of ligated THF molecules).

x	$(thf)_xMg(Carb)Br$		$(thf)_xMg(Carb)_2$		$(thf)_xMgBr_2$	
	E_{HOMO}	E_{LUMO}	E_{HOMO}	E_{LUMO}	E_{HOMO}	E_{LUMO}
1	−6.34	−0.62	−6.01	−0.64	−8.28	−0.22
2	−5.88	−0.13	−5.91	−0.22	−7.69	0.61
3	−5.74	−0.06	−5.79	−0.15	−7.31	0.78
4	−5.63	0.08	–	–	−6.81	0.89

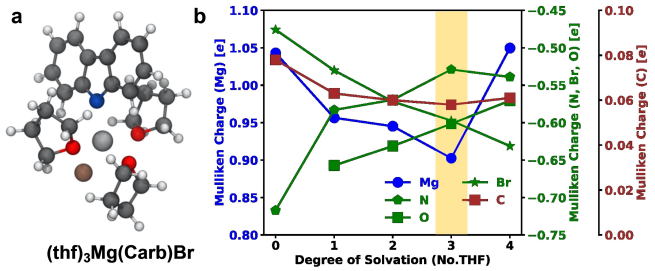

Figure 4. (a) Molecular structure of $(thf)_3Mg(Carb)Br$ calculated with DFT. (b) Respective Mulliken charges for Mg, N, Br, O and C at different solvation degrees. The charges for O are averaged over the oxygen atoms of the THFs. The same applies to the charges of the C atoms, which are averaged over the carbon atoms of the carbazolyl group. The yellow area marks the most probable degree of solvation according to NMR. Number of ligated THF molecules is in perfect agreement with NMR results. Calculated bond lengths of $(thf)_3Mg(Carb)Br$ (DFT) are also in agreement with X-ray structure results (pm): Mg1–N1 203.6, Mg1–Br1 247.3, Mg1–O1 216.5, Mg1–O2 210.8, Mg1–O3 219.6; bond angles (deg.) at Mg1: N1–Mg1–Br1 127.0, N1–Mg1–O1 88.4, N1–Mg1–O2 126.8, N1–Mg1–O3 91.5, O1–Mg1–O2 82.3, O1–Mg1–O3 166.7, O1–Mg1–Br1 94.4, O2–Mg1–O3 87.2, O2–Mg1–Br1 105.9, O3–Mg1–Br1 96.2.

degree of solvation is also associated with steric effects. In case of the bromine ligand in $(thf)_xMg(Carb)Br$, the Mg–Br bond increases (232.3 < 236.4 < 241.6 < 247.3 < 262.5 pm, for x = 0–4), resulting in about 10% less charge being transferred from bromine to magnesium per additional THF molecule. The Mg–N bond distance also increases upon solvation (192.4 < 198.0 < 199.8 < 203.6 < 212.1 pm, for x = 0–4), although the negative charge on the nitrogen atom decreases ($-0.71e < -0.58e < -0.57e < -0.53e < -0.52e$, for x = 0–4). The free-electron pairs of the THF oxygen atoms cause a negative charge transfer from the nitrogen electrons into the aromatic system of the carbazolyl group due to electrostatic repulsions. That is consistent with the averaged positive charge on the aromatic carbon atoms decreasing by approximately 10% with the first THF molecule and an additional 4% with each subsequent THF molecule. The charge on the magnesium cation remains largely constant but shows a minimum positive charge in the trigonal bipyramidal structure, which was experimentally determined by NMR spectroscopy. For the sake of completeness, the Mulliken charges of homoleptic $(thf)_xMg(Carb)_2$ and $(thf)_xMgBr_2$ may be found in the Supporting Information (Figure S22, Figure S23, and Table S3).

Conclusion

The *in-situ* Grignard metalation method (*i*GMM) of carbazole, i.e. the metalation of carbazole by Mg in the presence of ethyl bromide in THF, allows to prepare the slightly green Hauser base $[(thf)_3Mg(Carb)Br]$ (**1**) which is only sparingly soluble. A Schlenk-type equilibrium is operative leading to the formation of homoleptic $[(thf)_3Mg(Carb)_2]$ and $[(thf)_4MgBr_2]$. Quantum chemical calculations show preferred coordination numbers and increasing solvation energies in the series $(thf)_xMgBr_2 < (thf)_xMg(Carb)Br < (thf)_xMg(Carb)_2$ for an equal number x of ligated THF molecules. If the *i*GMM is performed in the presence of lithium halide, the heterobimetallic turbo-Hauser bases $[(thf)(Carb)Mg(\mu\text{-}Br/X)_2Li(thf)_2]$ (X = Br (**2**) and Cl (**3**)) form as has been verified by DOSY NMR spectroscopy. A THF solution of **1** shows a low over-potential and a good cyclability of electro-deposition/-stripping of Mg on a Cu current collector. An improved performance is achieved with the heterobimetallic turbo-Hauser bases $[(thf)(Carb)Mg(\mu\text{-}Br/Cl)_2Li(thf)_2]$.

Experimental Section

General information. All manipulations were carried out under an inert nitrogen atmosphere using standard Schlenk techniques, if not otherwise stated. The solvents were dried over KOH and subsequently distilled over sodium/benzophenone under a nitrogen atmosphere prior to use. All substrates were purchased from Alfa Aesar, abcr, Sigma Aldrich or TCI and used without further purification. The yields given are not optimized. Purity of the compounds was verified by NMR spectroscopy. Deuterated solvents were dried over sodium, distilled, degassed, and stored under nitrogen over sodium. ^{1}H, ^{29}Si and $^{13}C\{^{1}H\}$ NMR spectra were recorded on Bruker Avance III 400 (BBO, BBFO probes), Avance III HD 500 (BBO Prodigy probe) or Avance III HD 600 (TCI cryo probe) spectrometers. Chemical shifts are reported in parts per million relatively to $SiMe_4$ (^{1}H, ^{13}C) as an external standard referenced to the solvents residual proton signal using xiref AU program for ^{7}Li-NMR spectra. DOSY-NMR spectra were measured using the ledbpgp2 s standard pulse sequence. Molar masses in solution were calculated using the ECC-DOSY method.[22] ASAP-HSQC-spectra and ASAP-HSQC-DEPT-spectra were recorded using the published pulse sequences.[23]

*Synthesis of [(thf)$_3$CarbMgBr] (**1**).* Carbazole (4.93 g, 29.6 mmol, 1 eq.) and magnesium granules (0.79 g, 32.6 mmol, 1.1 eq.) were suspended in THF (60 mL). EtBr (2.22 mL, 6.0 mmol, 1 eq.) was added dropwise over 30 minutes and the reaction mixture was stirred at room temperature for 2 h. Titration of a hydrolysed aliquot with sulfuric acid (0.1 N) against phenolphthalein showed 88% yield. Almost after completion of the reaction the product crystallized spontaneously. The precipitate was collected by filtration (G3 frit) and dried under reduced pressure. $[(thf)_3MgCarbBr]$ (11.96 g, 24,3 mmol, 82%) was obtained as slightly green blocks. IR (ATR): 2981 (w), 2892 (w), 1619(w), 1493 (m), 1294 (m), 911 (m) cm^{-1}, m.p. = 138–143 °C. In $[D_8]$THF solution a Schlenk-type equilibrium was observed. *Physical data of [(thf)$_3$Mg(Carb)Br] (**1**):* ^{1}H NMR ($[D_8]$THF, 297 K, 400 MHz): δ = 8.00 (d, J = 7.64 Hz, 2H), 7.73 (d, J = 8.16 Hz, 2H), 7.20 (t, J = 7.54 Hz, 2H), 6.92 (t, J = 7.33 Hz, 2H) ppm, ^{13}C NMR ($[D_8]$THF, 297 K, 101 MHz): δ = 150.0, 123.0, 119.0, 114.6, 113.6, ^{1}H DOSY ($[D_8]$THF, 297 K, 400 MHz): $D_{Ref,THF} = 2.43 \cdot 10^{-9}$ m^2/s, $D_{[(thf)4MgCarbBr} = 7.42 \cdot 10^{-10}$ m^2/s, $MW_{calc} = 590$ g mol^{-1}, $MW_{found} = 589$ g mol^{-1}, Δ = 0%. *Physical data of [(thf)MgCarb$_2$]:* ^{1}H NMR

([D_8]THF, 297 K, 400 MHz): δ = 8.09 (d, J = 7.68 Hz, 2H), 7.60 (d, J = 8.20 Hz, 2H), 7.15 (t, J = 7.44 Hz, 2H), 6.97 (t, J = 7.30 Hz, 2H) ppm, ^{13}C NMR ([D_8]THF, 297 K, 101 MHz): δ = 150.0, 119.2, 118.4, 114.9, 114.0 ppm, ^{1}H DOSY ([D_8]THF, 297 K, 400 MHz): $D_{Ref,THF}$ = $2.43 \cdot 10^{-9}$ $m^2 s^{-1}$, $D_{[(thf)MgCarb2}$ = $8.50 \cdot 10^{-10}$ $m^2 s^{-1}$, MW_{calc} = 436 g mol^{-1}, MW_{found} = 467 g mol^{-1}, Δ = −7 %.

*Synthesis of [(thf)CarbMg(μ-Cl/Br)$_2$Li(thf)$_2$] (**2**).* NMR-scale: Carbazole (20 mg, 120 μmol,1 eq.), magnesium turnings (3 mg, 120 μmol, 1 eq.) and LiCl (4 mg, 0.8 eq. 96 μmol) were suspended in 550 μL of [D_8]THF. EtBr (9 μL, 1 eq.) was added, and the Young tube was sealed. After a few minutes gas evolution was observed and after 3 h gas evolution ceased. During this time, a yellow-green solution formed. Physical data of **2**: ^{1}H NMR ([D_8]THF, 233 K, 400 MHz): δ = 7.95, (d, J = 6.3 Hz, 4H), 7.07 (t, J = 7.36, 8.94 Hz, 2H), 6.81 (t, J = 6.84, 9.47 Hz, 2H) ppm, ^{13}C NMR ([D_8]THF, 233 K, 101 MHz): δ = 150.7, 122.2, 118.4, 115.9, 113.7 ppm, ^{7}Li NMR ([D_8]THF, 233 K, 155.5 MHz): δ = −0.05 (s) ppm, ^{1}H DOSY ([D_8]THF, 297 K, 400 MHz): $D_{Ref,THF}$ = $2.19 \cdot 10^{-9}$ $m^2 s^{-1}$, $D_{[(thf)CarbMg-μ-Cl,Br-Li(thf)2]}$ = $7.02 \cdot 10^{-10}$ $m^2 s^{-1}$, MW_{calc} = 553 g mol^{-1}, MW_{found} = 539 g mol^{-1}, Δ = 2 %.

*Synthesis of [(thf)CarbMg-μ-Br$_2$-Li(thf)$_2$] (**3**).* LiBr (1.58 g, 18,19 mmol, 1 eq.), Mg granules (440 mg, 18.19 mmol, 1 eq.) and carbazole (3.04 g, 18.19 mmol, 1 eq.) were suspended in 30 mL of THF and cooled to 10 °C. EtBr (1.4 mL, 18.19 mmol, 1 eq.) was added in two portions and the reaction mixture was stirred for 2 h at room temperature. Physical data of **3**: ^{1}H NMR ([D_8]THF, 297 K, 400 MHz): δ = 7.93 (d, J = 7.7 Hz, 1H), 7.86 (d, J = 8.2 Hz, 1H), 7.19–7.07 (m, 1H), 6.90–6.80 (m, 1H), 3.65 (s, THF), 1.79 (s, THF) ppm, ^{13}C NMR ([D_8]THF, 297 K, 101 MHz): δ = 150.2, 125.1, 124.9, 122.7, 119.7, 118.6, 118.3, 114.2, 114.2, 110.5 ppm, ^{7}Li NMR ([D_8]THF, 297 K, 155.5 MHz): δ = 0.35 ppm, ^{1}H DOSY ([D_8]THF, 297 K, 400 MHz): $D_{Ref,Si(SiMe3)4}$ = $9.39 \cdot 10^{-10}$ $m^2 s^{-1}$, $D_{[(thf)CarbMg-μ-Br2-Li(thf)2]}$ = $6.37 \cdot 10^{-10}$ $m^2 s^{-1}$, MW_{calc} = 573 g mol^{-1}, MW_{found} = 581 g mol^{-1}, Δ = 1 %.

Crystal Structure Determination of 1. The intensity data for **1** were collected on a Nonius KappaCCD diffractometer using graphite-monochromated Mo-$K_α$ radiation. Data were corrected for Lorentz and polarization effects; absorption was taken into account on a semi-empirical basis using multiple-scans.[24–26] The structures were solved by direct methods (SHELXS[27]) and refined by full-matrix least squares techniques against F_o^2 (SHELXL-2018).[28] All hydrogen atoms were located by difference Fourier synthesis and refined isotropically. All non-hydrogen atoms were refined anisotropically.[28] The program packages XP[29] and POV-Ray[30] were used for structure representations. Crystal and refinement data for **1**: $C_{24}H_{32}BrMgNO_3$, M = 486.72 g mol^{-1}, colorless prism, size 0.108 × 0.102 × 0.088 mm^3, monoclinic, space group $P2_1/n$, a = 11.3856(2), b = 14.5083(4), c = 14.3729(4) Å, β = 107.130(1)°, V = 2268.88(10) Å^3, T = −140 °C, Z = 4, $ρ_{calcd.}$ = 1.425 g cm^{-3}, μ (Mo-$K_α$) = 18.65 cm^{-1}, multi-scan, $trans_{min}$: 0.6939, $trans_{max}$: 0.7456, F(000) = 1016, 16569 reflections in h(−14/14), k(−18/18), l(−18/18), measured in the range 2.042° ≤ Θ ≤ 27.484°, completeness Θmax = 99.8 %, 5171 independent reflections, R_{int} = 0.0573, 4228 reflections with $F_o > 4σ(F_o)$, 399 parameters, 0 restraints, $R1_{obs}$ = 0.0484, wR^2_{obs} = 0.1002, $R1_{all}$ = 0.0646, wR^2_{all} = 0.1091, GOOF = 1.078, largest difference peak and hole: 0.588/−0.625 e Å^{-3}.

Electrochemical Characterization. Copper foil (99.95 %, *thickness* = 0.01 mm, Schlenk), magnesium foil (99.95 %, *thickness* = 0.15 mm, Goodfellow) and magnesium wire (99.99 %, *d* = 1 mm, Goodfellow) were used as working, counter and reference electrodes, respectively. Prior to use, the copper foil was dried under vacuum at 120 °C. To remove the thin native oxide layer from the magnesium current collector the surface was polished with sandpaper (1200 micron). The electrochemical measurements were performed inside a glovebox in a three-electrode configuration using EL-Cell ECC-Ref cells conducted to a BioLogic VMP3 potentiostat. Magnesium and Copper foil used as counter and working electrode (*d* = 18 mm) and a piece of magnesium wire was used as reference electrode, respectively. A glass fiber used as separator (1.55 mm thick, ECC-01-0021-C/L, EL-Cell) used as reservoir for Mg electrolyte (450 μL). Cyclic voltammetry experiments were run in a potential range between −0.8 V to 1.8 V *vs.* Mg/Mg^{2+} at a scan rate of 10 mV s^{-1}. Mg was electro-deposited onto copper current collector using chronopotentiometry at a fixed current density of −0.6 mA cm^{-2}.

Ex-situ Analysis. X-ray diffraction (XRD) and scanning electron microscopy (SEM) were applied to characterize the morphology of the electrodeposited Mg on the current collector. XRD pattern was recorded using an air-dome sample holder in a single scan between 10° and 90° in 0.02° 2θ increments on a Bruker AXS D8 Discover using Cu–Kα radiation, a Ni-monochromator and a LYNXEYE 2D energy dispersive detector. The SEM images have been obtained with a LEO 1530 VP microscope with an acceleration of 5.0 kV and a secondary electron detector.

Computational Details. All electrolyte structures were generated using the Amsterdam Modelling Suite and pre-optimized with the semi-empirical MOPAC engine.[31] Spin unrestricted, non-relativistic first principle geometry optimizations were subsequently performed within the Amsterdam Density Functional (ADF) framework, using slater type orbitals (STOs) with a triple-ζ polarized (TZP), all-electron basis set and the meta hybrid exchange correlation functional MN15 as part of the LibXC library.[32] Convergence criteria were chosen to be $2.6 \cdot 10^{-3}$ kJ·mol^{-1} for the energy difference between two consecutive self-consistent field (SCF) cycles and 2.6 kJ·mol^{-1}·Å^{-1} for the forces during geometry optimization. The gain in solvation energy per additional THF $E_{solv,gain}$ was calculated for $(thf)_xMg(Carb)Br$, $(thf)_xMg(Carb)_2$, and $(thf)_xMgBr_2$ using equation 1, where x equals the number of coordinated THF solvent molecules.

$$E_{solv,\ gain} = E^{(thf)_x\text{Electrolyte}} - E^{(thf)_{(x-1)}\text{Electrolyte}} - E^{thf} \quad (1)$$

In addition, the cumulative solvation energy for a given conformation was determined by equation 2:

$$E_{solv,\ cum} = \sum_{(thf)_1}^{(thf)_x} E^{(thf)_x\text{Electrolyte}}_{solv,\ gain} \quad (2)$$

Atomic charges were obtained by the Mulliken charge analysis.[33]

Supporting Information (see footnote on the first page of this article)

Experimental details, analytical methods as well as NMR spectra and theoretical data (pdf format). Crystallographic data (excluding structure factors) has been deposited with the Cambridge Crystallographic Data Centre as supplementary publication CCDC-2142703 for **1**. Copies of the data can be obtained free of charge on application to CCDC, 12 Union Road, Cambridge CB2 1EZ, UK [E- mail: deposit@ccdc.cam.ac.uk].

Deposition Number 2142703 (for **1**) contains the supplementary crystallographic data for this paper. These data are provided free of charge by the joint Cambridge Crystallographic Data Centre and Fachinformationszentrum Karlsruhe Access Structures service www.ccdc.cam.ac.uk/structures.

Acknowledgements

We acknowledge the valuable support of the NMR service platform (www.nmr.uni-jena.de/) of the Faculty of Chemistry and Earth Sciences of the Friedrich Schiller University Jena, Germany. P. Schüler is very grateful to the German Environment Foundation (Deutsche Bundesstiftung Umwelt, DBU, grant no. 20018/578) for a generous Ph.D. grant. This work contributes to the research performed at CELEST (Center for Electrochemical Energy Storage Ulm-Karlsruhe) and was partly funded by the German Research Foundation (DFG) under Project ID 390874152 (POLiS Cluster of Excellence). The authors acknowledge support by the state of Baden-Württemberg through bwHPC and the German Research Foundation (DFG) through grant no INST 40/575-1 FUGG (JUSTUS 2 cluster). Open Access funding enabled and organized by Projekt DEAL.

Conflict of Interest

The authors declare no conflict of interest.

Data Availability Statement

The data that support the findings of this study are available in the supplementary material of this article.

Keywords: Batteries · Electrolytes · Hauser bases · Magnesium · Structure elucidation · Turbo-Hauser bases

[1] a) C. R. Hauser, H. G. Walker, *J. Am. Chem. Soc.* **1947**, *69*, 295–297; b) C. R. Hauser, C. R. Hance, *J. Am. Chem. Soc.* **1951**, *73*, 5846–5848.
[2] a) B. Haag, M. Mosrin, H. Ila, V. Malakhov, P. Knochel, *Angew. Chem. Int. Ed.* **2011**, *50*, 9794–9824; *Angew. Chem.* **2011**, *123*, 9968–9999; b) A. Kremsmair, J. H. Harenberg, K. Schwärzer, A. Hess, P. Knochel, *Chem. Sci.* **2021**, *12*, 6011–6019.
[3] a) K.-C. Yang, C.-C. Chang, J.-Y. Huang, C.-C. Lin, G.-H. Lee, Y. Wang, M. Y. Chiang, *J. Organomet. Chem.* **2002**, *648*, 176–187; b) P. García-Álvarez, D. V. Graham, E. Hevia, A. R. Kennedy, J. Klett, R. E. Mulvey, C. T. O'Hara, *Angew. Chem. Int. Ed.* **2008**, *47*, 8079–8081; *Angew. Chem.* **2008**, *120*, 8199–8201.
[4] a) A. S. Batsanov, P. D. Bolton, R. C. B. Copley, M. G. Davidson, J. A. K. Howard, C. Lustig, R. D. Price, *J. Organomet. Chem.* **1998**, *550*, 445–448; b) D. R. Armstrong, P. Garcá-Álvarez, A. R. Kennedy, R. E. Mulvey, J. A. Parkinson, *Angew. Chem. Int. Ed.* **2010**, *49*, 3185–3188; *Angew. Chem.* **2010**, *122*, 3253–3256.
[5] R. Neufeld, T. L. Teuteberg, R. Herbst-Irmer, R. A. Mata, D. Stalke, *J. Am. Chem. Soc.* **2016**, *138*, 4796–4806.
[6] Selected recent examples demonstrate the scope of these turbo-Hauser bases: a) A. Castelló-Micó, J. Nafe, K. Higashida, K. Karaghiosoff, M. Gingras, P. Knochel, *Org. Lett.* **2017**, *19*, 360–363; b) M. Balkenhohl, R. Greiner, I. S. Makarov, B. Heinz, K. Karaghiosoff, H. Zipse, P. Knochel, *Chem. Eur. J.* **2017**, *23*, 13046–13050; c) A. Castelló-Micó, P. Knochel, *Synthesis* **2018**, *50*, 155–169; d) M. Balkenhohl, B. Salgues, T. Hirai, K. Karaghiosoff, P. Knochel, *Org. Lett.* **2018**, *20*, 3114–3118; e) M. Baenziger, S. Eswaran, Y. Jiang, G. Kasinathan, *Synthesis* **2019**, *51*, 1649–1654; f) K. Schwärzer, C. P. Tüllmann, S. Graßl, B. Górski, C. E. Brocklehurst, P. Knochel, *Org. Lett.* **2020**, *22*, 1899–1902.
[7] R. Neufeld, D. Stalke, *Chem. Eur. J.* **2016**, *22*, 12624–12628.
[8] R. L.-Y. Bao, R. Zhao, L. Shi, *Chem. Commun.* **2015**, *51*, 6884–6900.
[9] S. Dongmo, S. Zaubitzer, P. Schüler, S. Krieck, L. Jörissen, M. Wohlfahrt-Mehrens, M. Westerhausen, M. Marinaro, *ChemSusChem* **2020**, *13*, 3530–3538.
[10] M. Mao, T. Gao, S. Hou, C. Wang, *Chem. Soc. Rev.* **2018**, *47*, 8804–8841.
[11] J. Muldoon, C. B. Bucur, T. Gregory, *Chem. Rev.* **2014**, *114*, 11683–11720.
[12] M. Marinaro, D. Bresser, E. Beyer, P. Faguy, K. Hosoi, H. Li, J. Sakovica, K. Amine, M. Wohlfahrt-Mertens, S. Passerini, *J. Power Sources* **2020**, *459*, 228073.
[13] A. Mauger, C. M. Julien, *Inorganics* **2022**, *10*, 5.
[14] a) M. Armand, J.-M. Tarascon, *Nature* **2008**, *451* (7179), 652–657; b) M. R. Palacin, *Acc. Mater. Res.* **2021**, *2*, 319–326.
[15] a) D. Aurbach, Z. Lu, A. Schechter, Y. Gofer, H. Gizbar, R. Turgemann, Y. Cohen, *Nature* **2000**, *407* (6805), 724–727; b) H. S. Kim, T. S. Arthur, G. D. Allred, J. Zajicek, J. G. Newman, A. E. Rodnyansky, A. G. Oliver, W. C. Boggess, J. Muldoon, *Nat. Commun.* **2011**, *2* (1), 426–427; c) R. Dominiko, J. Bitenc, R. Berthelot, M. Gauthier, G. Pagot, V. Di Noto, *J. Power Sources* **2020**, *478*; d) Y. Liang, H. Dong, D. Aurbach, Y. Yao, *Nat. Energy* **2020**, *5* (9), 646–656; e) Q. Guo, W. Zeng, S.-L. Liu, Y.-Q. Li, J.-Y. Xu, Y. Wang, *Rare Met.* **2021**, *40* (2), 290–308; f) F. Maroni, S. Dongmo, C. Gauckler, M. Marinaro, M. Wohlfahrt-Mertens, *Batteries & Supercaps* **2021**, *4*, 1–32.
[16] S. Krieck, P. Schüler, J. M. Peschel, M. Westerhausen, *Synthesis* **2019**, *51*, 1115–1122.
[17] a) Z. Zhao-Karger, M. Gil Bardaji, O. Fuhr, M. Fichtner, *J. Mater. Chem. A* **2017**, *5* (22), 10815–10820; b) K. Sato, G. Mori, T. Kiyosu, T. Yaji, K. Nakanishi, T. Otha, K. Okamoto, Y. Orikasa, *Sci. Rep.* **2020**, *10* (1), 7362.
[18] A. Ponrouch, M. R. Palacín, *Phil. Trans. R. Soc. A* **2019**, *377*, 20180297.
[19] a) K. Tang, A. Du, S. Dong, Z. Cui, X. Liu, C. Lu, J. Zhao, X. Zhou, G. Cui, *Adv. Mater.* **2020**, *32* (6), 1904987; b) S. S. Kim, K. A. See, *ACS Appl. Mater. Interfaces* **2021**, *13* (1), 671–680.
[20] H. E. Swanson, E. Tatge, *Natl. Bur. Stand. Rep.* **1953**, (ICDD PDF No. 00–004-0770).
[21] a) Z. Li, O. Fuhr, M. Fichtner, Z. Zhao-Karger, *Energy Environ. Sci.* **2019**, *12*, 3496–3501; b) A. J. Crowe, K. K. Stringham, B. M. Bartlett, *ACS Appl. Mater. Interfaces* **2016**, *8*, 23060–23065; c) W. Ren, D. Wu, Y. NuLi, D. Zhang, Y. Yang, Y. Wang, J. Yang, J. Wang, *ACS Energy Lett.* **2021**, *6*, 3212–3220.
[22] R. Neufeld, D. Stalke, *Chem. Sci.* **2015**, *6*, 3354–3364.
[23] a) D. Schulze-Sünnighausen, J. Becker, B. Luy, *J. Am. Chem. Soc.* **2014**, *136*, 1242–1245; b) D. Schulze-Sünnighausen, J. Becker, M. R. M. Koos, B. Luy, *J. Magn. Reson.* **2017**, *281*, 151–161.
[24] R. Hooft: COLLECT, Data Collection Software; Nonius B. V., Netherlands, **1998**.
[25] Z. Otwinowski, W. Minor, in *Methods in Enzymology* (Eds. C. W. Carter, R. M. Sweet), vol. *276*, part A, Academic Press, San Diego, USA, **1997**, pp. 307–326.
[26] L. Krause, R. Herbst-Irmer, G. M. Sheldrick, D. Stalke, *J. Appl. Crystallogr.* **2015**, *48*, 3–10.
[27] G. M. Sheldrick, *Acta Crystallogr. Sect. A* **2015**, *71*, 3–8.
[28] G. M. Sheldrick, *Acta Crystallogr. Sect. C* **2015**, *71*, 3–8.
[29] XP, Siemens Analytical X-ray Instruments Inc., Karlsruhe, Germany, **1990**; Madison, WI, USA, **1994**.
[30] POV-Ray, Persistence of Vision Raytracer, Victoria, Australia, **2007**.
[31] a) AMS 2020, SCM, Theoretical Chemistry, Vrije Universiteit, Amsterdam, The Netherlands, http://www.scm.com. **2020**; b) J. J. P. Stewart, *J. Mol. Model.* **2013**, *19*, 1–32; c) AMS 2020 MOPAC: MOPAC Engine based on the MOPAC2016 source code (J. P. James, http://OpenMOPAC.net).
[32] a) G. te Velde, F. M. Bickelhaupt, E. J. Baerends, C. Fonseca Guerra, S. J. A. van Gisbergen, J. G. Snijders, T. Ziegler, *J. Comput. Chem.* **2001**, *22*, 931–967; b) ADF 2020, SCM, Theoretical Chemistry, Vrije Universiteit, Amsterdam, The Netherlands, http://www.scm.com. **2020**; c) D. P. Chong, E. Van Lenthe, S. Van Gisbergen, E. J. J. Baerends, *Comput. Chem.* **2004**, *25*, 1030–1036; d) H. S. Yu, X. He, S. L. Li, D. G. Truhlar, *Chem. Sci.* **2016**, *7*, 5032–5051; e) S. Lehtola, C. Steigemann, M. J. T. Oliveira, M. A. L. Marques, *SoftwareX* **2018**, *7*, 1–5.
[33] R. S. Mulliken, *J. Chem. Phys.* **1955**, *23*, 1833–1840.

Manuscript received: March 9, 2022
Revised manuscript received: March 15, 2022
Accepted manuscript online: March 16, 2022

RESEARCH ARTICLE

Lithium-ion batteries show excellent performance but pose challenges at the same time related to the accessibility of lithium metal. Therefore, alternatives based on magnesium are very attractive and the electrolytes must fulfill specific requirements like non-corrosiveness and electrochemical stability as well as straightforward synthesis. The carbazolylmagnesium halide system offers a promising strategy for a suitable Mg-based electrolyte.

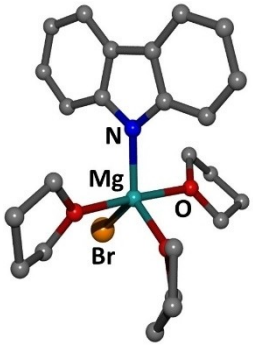

*P. Schüler, S. Sengupta, S. Zaubitzer, F. Fiesinger, Dr. S. Dongmo, Dr. H. Görls, Dr. M. Wohlfahrt-Mehrens, M. van den Borg, D. Gaissmaier, Dr. S. Krieck, Dr. M. Marinaro, T. Jacob, Prof. Dr. M. Westerhausen**